Effects of neuromyelitis optica–IgG at the blood–brain barrier in vitro

OPEN

Yukio Takeshita, MD, PhD
Birgit Obermeier, PhD
Anne C. Cotleur, MS
Simona F. Spampinato, MD, PhD
Fumitaka Shimizu, MD, PhD
Erin Yamamoto, BA
Yasuteru Sano, MD, PhD
Thomas J. Kryzer, AS
Vanda A. Lennon, MD
Takashi Kanda, MD, PhD
Richard M. Ransohoff, MD

Correspondence to Dr. Ransohoff: richard.ransohoff@biogen.com

ABSTRACT

Objective: To address the hypothesis that physiologic interactions between astrocytes and endothelial cells (EC) at the blood–brain barrier (BBB) are afflicted by pathogenic inflammatory signaling when astrocytes are exposed to aquaporin-4 (AQP4) antibodies present in the immunoglobulin G (IgG) fraction of serum from patients with neuromyelitis optica (NMO), referred to as NMO-IgG.

Methods: We established static and flow-based in vitro BBB models incorporating co-cultures of conditionally immortalized human brain microvascular endothelial cells and human astrocyte cell lines with or without AQP4 expression.

Results: In astrocyte–EC co-cultures, exposure of astrocytes to NMO-IgG decreased barrier function, induced CCL2 and CXCL8 expression by EC, and promoted leukocyte migration under flow, contingent on astrocyte expression of AQP4. NMO-IgG selectively induced interleukin (IL)-6 production by AQP4-positive astrocytes. When EC were exposed to IL-6, we observed decreased barrier function, increased CCL2 and CXCL8 expression, and enhanced leukocyte transmigration under flow. These effects were reversed after application of IL-6 neutralizing antibody.

Conclusions: Our results indicate that NMO-IgG induces IL-6 production by AQP4-positive astrocytes and that IL-6 signaling to EC decreases barrier function, increases chemokine production, and enhances leukocyte transmigration under flow. ***Neurol Neuroimmunol Neuroinflamm* 2017;4: e311; doi: 10.1212/NXI.0000000000000311**

GLOSSARY

AM = astrocyte medium; **AQP4** = aquaporin-4; **BBB** = blood–brain barrier; **BDNF** = brain-derived neurotrophic factor; **EC** = endothelial cell; **ESAM** = endothelial cell–selective adhesion molecule; **GDNF** = glial cell line–derived neurotrophic factor; **GFAP** = glial fibrillary acidic protein; **IFN** = interferon; **IgG** = immunoglobulin G; **IL** = interleukin; **NMO** = neuromyelitis optica; **PBMC** = peripheral blood mononuclear cells; **PDGF** = platelet-derived growth factor; **qRT-PCR** = quantitative reverse transcription polymerase chain reaction; **sIL-6R** = soluble interleukin-6 receptor; **TGF- β** = transforming growth factor–β; **VEGF** = vascular endothelial growth factor.

Neuromyelitis optica (NMO) is a severe autoimmune astrocytopathy with widespread but distinctive lesions.[1,2] Florid necrotizing inflammatory pathology is typified by astrocyte loss, immunoglobulin and complement deposition, and infiltration of neutrophils, mononuclear phagocytes, and eosinophils. In contrast, lesions lacking complement activation are often sublytic, featuring reactive astrocytes and selective loss of the water channel aquaporin-4 (AQP4). NMO was considered a subtype of multiple sclerosis due to overlapping clinical manifestations and the relapsing nature of both diseases[3,4] until a serum biomarker termed NMO–immunoglobulin G (IgG), containing antibodies against AQP4, allowed discrimination.[5–7]

Editorial, page XXX

Supplemental data at Neurology.org/nn

From the Neuroinflammation Research Center (Y.T., B.O., A.C.C., S.F.S., F.S., E.Y., R.M.R.), Lerner Research Institute, Cleveland Clinic, OH; Department of Neurology and Clinical Neuroscience (Y.S., T.K.), Yamaguchi University Graduate School of Medicine, Japan; and Department of Laboratory Medicine and Pathology (T.J.K., V.A.L.), Mayo Clinic, Rochester, MN. Y.T. and F.S. are currently affiliated with the Department of Neurology and Clinical Neuroscience, Yamaguchi University Graduate School of Medicine, Japan. B.O., A.C.C., and R.M.R. are currently affiliated with Neuroimmunology Research, Biogen, Cambridge, MA. S.F.S. is currently affiliated with the Department of Biomedical and Biotechnological Sciences, Section of Pharmacology, University of Catania, Italy.

Funding information and disclosures are provided at the end of the article. Go to Neurology.org/nn for full disclosure forms. The Article Processing Charge was paid by the authors.

NMO-IgG exhibits a distinctive perivascular binding pattern on rodent brain tissue sections incubated with serum from patients with NMO,[6] consistent with reactivity against AQP4 expressed on astrocyte perivascular endfeet.[8,9] NMO-IgG induces complement-dependent astrocytic cell toxicity and the production of inflammatory mediators, raising the possibility that reactive astrocytes precede and promote destructive inflammation in NMO.[10]

Patients with NMO occasionally manifest posterior reversible encephalopathy, indicating vascular dysfunction.[11] Diffuse vascular pathology along with blood–brain barrier (BBB) disruption is also found at various disease stages. Since astrocyte–endothelial cell (EC) signaling supports barrier function, it is reasonable to propose that AQP4-IgG, when binding to astrocytes, could disrupt this interaction. Indeed, AQP4-IgG increased permeability and cellular migration across a BBB model due to complement-dependent astrocytopathy.[12,13] However, it remains unclear how AQP4-IgG in the absence of complement contributes to BBB breakdown.[14]

Our results from using a human flow-based EC/astrocyte co-culture BBB model[15] suggest a mechanism by which AQP4-IgG binds to astrocytes, and indirectly disrupts EC function, accelerating inflammatory tissue injury.

METHODS

Standard protocol approvals, registrations, and patient consents. All study protocols were approved by the Cleveland Clinic and signed informed consent was obtained from all healthy donors whose blood samples were used in transmigration assays. The provision of de-identified patients' serum specimens, and IgG fractions thereof, for collaborative study at the Cleveland Clinic was approved by the Mayo Clinic Institutional Review Board. Signed informed consent was waived.

Immunohistochemical reagents. IgGs specific for AQP4 (rabbit polyclonal; Santa Cruz Biotechnology, Dallas, TX), Claudin 5 (rabbit polyclonal; Abcam, Cambridge, UK), glial fibrillary acidic protein (GFAP) (mouse monoclonal; Covance, Princeton, NJ), human CD126 (mouse monoclonal; US Biological, Salem, MA), TO-PRO-3 (Life Technologies, Carlsbad, CA), recombinant human interleukin (IL)–6 (R&D Systems, Minneapolis, MN), human soluble IL-6 receptor (sIL-6R; ProSpec, Ness-Ziona, Israel), and Alexa Fluor 488 Phalloidin (Life Technologies) were used in these experiments.

Cell culture. ECs are adult human brain microvascular ECs immortalized with temperature-sensitive SV40-LT as described.[16] ECs were grown in MCDB131 medium (Sigma-Aldrich, St. Louis, MO) supplemented with EGM-2 SingleQuot Kit Suppl. & Growth Factors (Lonza, Basel, Switzerland), 20% heat-inactivated fetal bovine serum, 100 U/mL penicillin (Sigma-Aldrich), and 100 μg/mL streptomycin (Sigma-Aldrich).

Astrocytes (A) and astrocytes transfected to express AQP4 M23 isoform (A4) were grown in astrocyte medium (AM; ScienCell, Carlsbad, CA) containing 2% heat-inactivated fetal bovine serum, astrocyte growth supplement, and penicillin/streptomycin solution (ScienCell). AM was used in all experiments when ECs were co-cultured with A or A4. A and A4 are well-characterized conditionally immortalized human astrocyte cell lines, which were previously reported.[17,18] A cells express AQP4 mRNA but undetectable amounts of AQP4 protein, unlike A4 cells, in which overexpression of AQP4 mRNA results in sufficient amounts of AQP4 protein that is not altered after several passages, equivalent to primary astrocytes.[18] When A and A4 were cultured at 37°C, their growth rate was lower than that observed at 33°C (figure e-1A at Neurology.org/nn). Doubling time at 33°C was similar between 2 cell lines (figure e-1A). Differentiated at 37°C, A4 and A were polygonal with numerous processes (figure e-1B). Both A and A4 expressed GFAP. A4, but not A, expressed cell-surface AQP4 (figure e-1B). Cells were expanded in a humidified atmosphere of 5% carbon dioxide/95% air at 33°C. Analyses were performed 1 or 2 days after the temperature shift to 37°C.

NMO-IgG and control IgG. Control IgG and NMO-IgG (50 patients with NMO) were prepared from surplus clinical serum specimens. IgG was isolated by affinity chromatography over protein G sepharose and dialyzed for use in these experiments. Preparations were carried out in a single laboratory (Department of Laboratory Medicine and Pathology, Mayo Clinic, Rochester, MN) using the same reagents, and protein concentrations were adjusted to ensure equivalence. We used IgGs at a final concentration of 400 μg/mL, the minimum needed for NMO-IgG to induce partial AQP4 internalization.

Immunocytochemistry. GFAP and Claudin 5 were detected by indirect immunocytochemistry on confluent ECs, A4, and A, as previously described.[18] Cells were not permeabilized when AQP4 antibody, NMO-IgG, and control IgG were used as primary antibodies. Cells were incubated overnight at 4°C with NMO-IgG (1 μg/mL) and control IgGs (1 μg/mL). As secondary antibodies, we used AlexaFluor 488 or 594 goat anti-rabbit IgG (Life Technologies: A-11008), AlexaFluor 488 goat anti-mouse IgG (Life Technologies: A-11001), and AlexaFluor 488 goat anti-human IgG (Life Technologies: A-11013). Slides were imaged using a laser scanning confocal microscope (SP5; Leica Microsystems, Newcastle, UK).

AQP4 live cell staining. NMO-IgG or control IgG (400 μg/mL) were added to A4 and A cultures. After 8 hours at 37°C, cells were washed and fixed, and AQP4 was detected using commercial AQP4 antibody (1:500).

IL-6 trans-signaling assay and blockade with IL-6 receptor-neutralizing antibody. Recombinant human IL-6 (10 ng/mL), sIL-6R (100 ng/mL), and mouse anti-human CD126 antibody (20 ng/mL) were incubated with ECs or ECs/A4 for 30 minutes for quantitative PCR analysis and for 24 hours for BBB permeability and transmigration assays.

Astrocyte/EC co-cultures on transwell inserts. A4 or A were cultured on one side (abluminal) of polycarbonate transwell tissue culture inserts with 3 μm pores (Corning, Manassas, VA). After allowing 1 hour for astrocytes to attach, the membrane was inverted and ECs were seeded on the other side (luminal) and cells were cultured for 3 days at 33°C. After temperature shift to 37°C, NMO-IgG or control IgG (400 μg/mL) was added to the abluminal aspect of the membrane (in contact with astrocytes) for 6 hours.

Quantitative PCR. ECs were harvested from the luminal side of Transwell EC/A or EC/A4 co-culture inserts, and total RNA was isolated from EC with RNeasy kit (Qiagen, Venlo, Netherlands) according to the manufacturer's protocol. Single-stranded cDNA was prepared from 20 ng total RNA with SuperScriptIII kit (Invitrogen, Carlsbad, CA). Gene expression was analyzed by real-time reverse transcription (RT)–PCR with a polymerase ready mix (LightCycler 480; SYBR Green I Master; Roche, Basel, Switzerland) and a thermal cycler (LightCycler; Roche Diagnostics). Melting curve analysis for amplified PCR products and amplicon visualization on 8% polyacrylamide gels confirmed amplification specificity. For relative quantification of gene expression, mRNA levels were normalized to EC-selective adhesion molecule (ESAM) in ECs, or β-actin in A and A4, using the comparative threshold cycle ($\Delta\Delta^{CT}$) method. To exclude contamination of astrocyte cDNA, we confirmed absence of GFAP and AQP4 messages in all EC samples. Reactions were performed in triplicate. Chemokines CXCL1, 2, 8, 10, 12, CCL2, and CCL5 were measured as target molecules. Primers are listed in table e-1A. In initial pilot studies, we assayed mRNA levels for 4 cytokines (IL-1b, IL-4, IL-6, interferon [IFN]–β), 10 chemokines (CCL2, CCL5, CCL7, CCL8, CCL20, CXCL1, CXCL8, CXCL10, CXCL12, CX3CL1), and 5 vasoactive growth factors (transforming growth factor–β [TGF- β], vascular endothelial growth factor [VEGF], platelet-derived growth factor [PDGF], brain-derived neurotrophic factor [BDNF], glial cell line–derived neurotrophic factor [GDNF]) using quantitative RT (qRT)–PCR in A4 or A monocultures incubated with NMO-IgG. Primers are listed in table e-1B.

ELISA. After incubating A4 and A with NMO-IgG or control IgG for 24 hours, IL-6 concentration was measured in triplicate samples using human IL-6 ELISA Max Deluxe kit, per manufacturer's protocol (BioLegend, San Diego, CA).

The Cleveland Clinic Institutional Review Board approved study protocols, and signed informed consents were obtained from blood donors. We recruited healthy volunteers, aged 20–50 years, not experiencing systemic infection, and excluded individuals taking nonsteroidal anti-inflammatory drugs. Peripheral blood mononuclear cells (PBMC) were isolated with lymphocyte separation medium (Mediatech, Manassas, VA). For transmigration assays, performed within 2 hours of phlebotomy, PBMC were resuspended at 10×10^6 cells in 30 mL TEM buffer (RPMI 1640 without phenol red + 1% bovine serum albumin + 25 mM HEPES) and stained with Calcein AM (Life Technologies) before perfusion into the chamber.

Transmigration assays under flow. Flow-based transmigration assays were performed as previously described.[15] The 3D flow chamber (C.B.S. Scientific, Del Mar, CA) consisted of a peristaltic pump, framed polycarbonate membranes with 3 μm pores containing endothelial cell/astrocyte co-cultures, and a flow chamber allowing transendothelial migration. The pump delivers programmable flow to multiple devices simultaneously. Membranes coated with rat tail collagen I solution (50 μg/mL) (BD Biosciences, East Rutherford, NJ) were rinsed with PBS and individually distributed in 12-well plates. A4 or A were seeded on the abluminal side of the membrane and, after allowing astrocytes to attach for 1 hour at 33°C, the membrane was flipped with tweezers. EC were seeded on the luminal side and co-cultured in AM for 2 days at 33°C, then for 1 day at 37°C. After membranes were mounted in flow chambers, 10×10^6 PBMC (total cells per assays) in 30 mL TEM (held in a 37°C water bath) were perfused through the chamber with a shear stress of 2.0 dyne/cm^2. Total assay time was 60 minutes. All chambers remained on a 37°C slide warmer for the duration of the assay. After PBMC perfusion, chambers were flushed with PBS to remove loose cells, maintaining the same shear stress as in the assay. Migrated PBMC were recovered from the chamber's bottom well. Cells attached to the abluminal side of the membrane and the bottom well of the chamber were removed by a quick rinse with 0.5 mM EDTA. Total numbers of migrated cells were determined by a hemocytometer.

Phenotyping of PBMC. Input and migrated cells were analyzed by flow cytometry. After collection, cells were fixed for 10 minutes in 1% paraformaldehyde at room temperature, washed in PBS/0.1 mM EDTA, followed by blocking in mouse IgG. Cells were labeled with anti-human CD45 efluor450, CD8a APC-efluor780 (eBiosciences, San Diego, CA), CD3 Alexa Fluor 647, CD14 BV605 (BioLegend, San Diego, CA), CD19 BV711, CD4 PE-CF594 (BD Biosciences), and CD16 PE (R&D Systems). Data were acquired on a BD LSRFortessa SORP flow cytometer running Diva6, and analyzed in FlowJo 9.7.5 (Tree Star, Ashland, OR).

Solute permeability with 10 kDa dextran. EC, A, and A4 were cultured to confluence on 24-well collagen-coated Transwell tissue culture inserts (3 μm pore size; Corning) at 37°C. Solute permeability was assessed using 10 kDa dextran-conjugated fluorescein isothiocyanate (1 mg/mL; Sigma-Aldrich) and fluorescence recovery in the lower chamber was measured after 20, 60, and 120 minutes using a SpectraMax M2e microplate reader (Molecular Devices, Sunnyvale, CA). Apparent permeability coefficients (P_{app} in cm/min) were calculated as follows:

$$P_{app} = V(dc/dt)/AC_0,$$

where dc/dt = dextran flux across the membrane; V (cm^3) = volume in the receiver side; A (cm^2) = surface area of insert; C_0 (mM) = initial donor-compartment dextran concentration.

Area fraction measurement of Claudin 5. Images acquired by confocal microscopy were analyzed with ImageJ (NIH, Bethesda, MD). Following the ImageJ users' guide, noise was removed after deletion of nonspecific signal. Binary images were created automatically. The area fraction (percentage of Claudin 5 immunoreactive area per total window area) is displayed.

Data analysis. One-way analysis of variance, followed by Tukey-Kramer multiple comparison procedure, was used for statistical analysis. Values of $p < 0.05$ were considered significant. Values are expressed as mean ± SEM.

RESULTS

NMO-IgG binds A4 cells but not A cells. First, we verified the presence of AQP4-IgG in NMO-IgG but not in control IgG. In fixed cell preparations, NMO-IgG bound to AQP4-expressing A4 cells (figure 1A), but not to A cells (figure 1B). Neither control nor NMO-IgG showed immunoreactivity with A cells (figure 1, A and B). Commercial AQP4-IgG staining of A4 cells served as positive control (figure 1A). In live unfixed, nonpermeabilized astrocytes, NMO-IgG induced internalization of surface AQP4, resulting in appearance of immunoreactive cytoplasmic vesicular structures, as reported by others both in tissue culture and brain sections[19] (figure 1C), while control IgG failed to affect AQP4 (figure 1C, right panel). Taken together, we confirmed that AQP4-IgGs

Figure 1 Binding of neuromyelitis optica (NMO)–immunoglobulin G (IgG) to human astrocyte cell lines

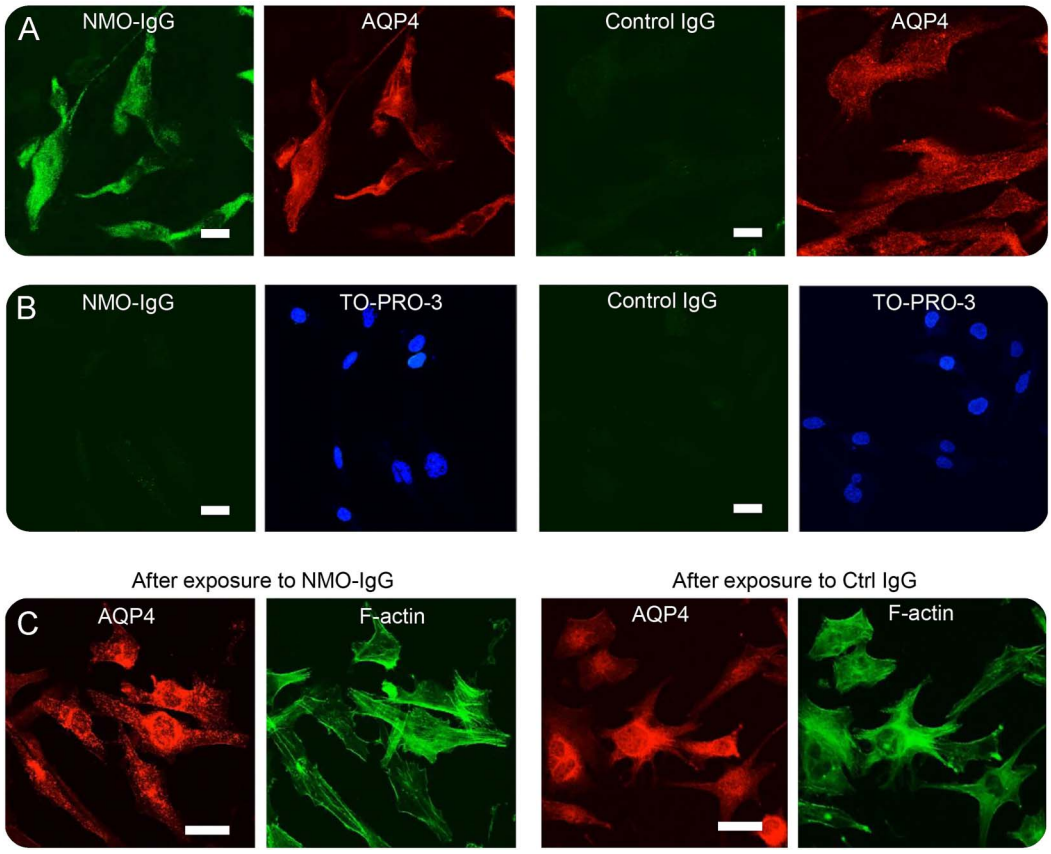

(A, B) Fixed cells were incubated with NMO-IgG (pooled from patient sera), control IgG (pooled from healthy donor sera), and commercial aquaporin-4 (AQP4) IgG (rabbit polyclonal, cytoplasmic epitopes). AlexaFluor 488 goat anti-human IgG was used to probe for bound NMO-IgG and control IgG, and AlexaFluor 594 goat anti-rabbit IgG to probe for commercial AQP4 IgG. (A: A4 cells; B: A cells). Nuclear counterstaining with TO-PRO-3 demonstrates the presence of cells in B. Scale bar, 10 μm. (C) Exposure of living A4 cells to NMO-IgG, but not to control IgG, leads to clustering/internalization of surface AQP4. Counterstaining with Phalloidin Alexa 488, after fixing and permeabilization, shows filamentous actin. Scale bar, 10 μm.

were present in our NMO-IgG preparation and bound AQP4 on A4 cells. Moreover, the NMO-IgG preparation induced AQP4 internalization in live-cell astrocyte stainings, as previously described by others using primary fetal rat astrocytes.[19] Control IgG showed no effect on fixed or on live astrocytes, validating this IgG preparation as a proper negative control. This evidence suggested that A4 cell line response to NMO-IgG resembles that of primary astrocytes.

Astrocytes exposed to NMO-IgG modulate barrier function of endothelial cells. Active NMO lesions are associated with profound BBB disruption indicated by intense gadolinium enhancement of MRI scans. To address mechanisms underlying this effect, we constructed in vitro EC/astrocyte co-cultures and exposed astrocytes (on the abluminal side) to NMO-IgG (figure 2A). Using low-molecular-weight dextran as a solute permeability probe, we found that BBB permeability coefficients increased in EC/A4 co-cultures exposed to NMO-IgG but not in cultures exposed to control IgG or in AQP4-negative A cells (figure 2B). We also observed no difference in solute permeability in ECs between EC/A and EC/A4 co-culture after incubation with control IgG (figure 2B), suggesting that the modulating properties for the 2 astrocyte cell lines on BBB function is comparable. To evaluate EC structural correlates of increased paracellular permeability, we examined Claudin 5 immunoreactivity. The area fraction of EC Claudin 5 expression was decreased in EC/A4 but not EC/A co-cultures after exposure of astrocytes to NMO-IgG but not control IgG (figure 2, C and D). These results indicated that exposure of A4 astrocytes to NMO-IgG on the abluminal side generated signals to luminal EC, resulting in decreased and discontinuous Claudin 5 immunoreactivity at interendothelial junctions and increased solute permeability.

Inflammatory cellular infiltrates are common at sites of BBB disruption and typify active NMO tissue lesions. After abluminal exposure to NMO-IgG, EC/A4 co-cultures showed a nearly 2-fold increase in the

Figure 2 **Effects of abluminal neuromyelitis optica (NMO)–immunoglobulin G (IgG) on barrier function of endothelial cells (EC)**

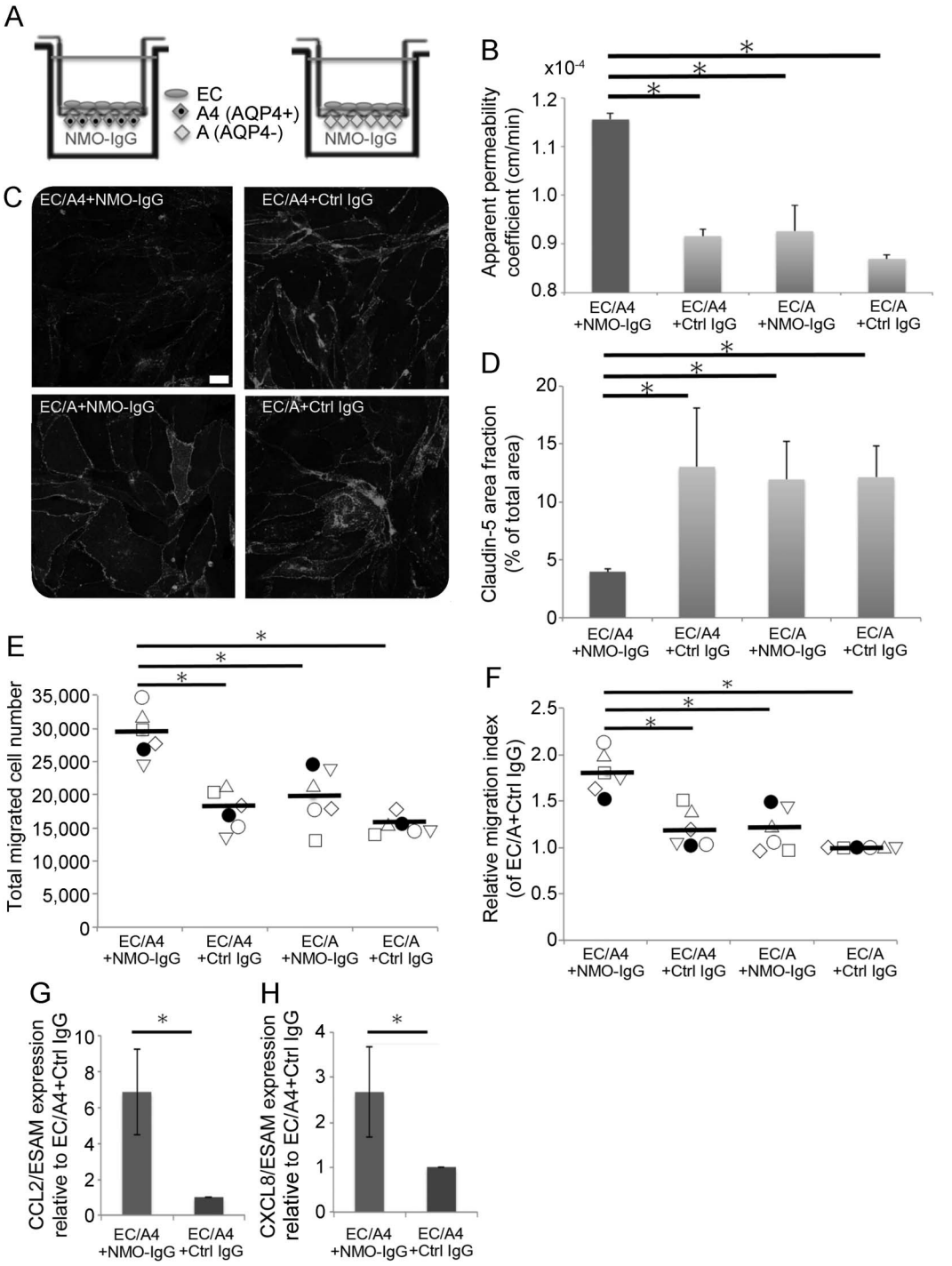

(A) Schematic depiction of each experimental condition, comprising EC co-cultured with either astrocytes positive (A4) or negative (A) for aquaporin-4 (AQP4) expression. NMO-IgG or control IgG was applied to the abluminal aspect of the in vitro blood-brain barrier (BBB), i.e., to the astrocyte side. (B) Effect of abluminal application of NMO-IgG on solute permeability to dextran 10k. Data are mean ± SEM with n = 5 replicates. *$p < 0.01$. (C) Addition of NMO-IgG to astrocytes reduces EC expression of Claudin 5. Scale bar, 10 μm. (D) Claudin 5 area fraction as determined from images represented in C. Data are mean ± SEM with n = 5 replicates. *$p < 0.01$. (E, F) Effects of abluminal application of NMO-IgG on peripheral blood mononuclear cells (PBMC) transmigration across an in vitro BBB under flow. In F, total migrated cell numbers (as reported in E) in each experiment were normalized to 1 using EC/A exposed to control IgG, and expressed as relative migration index. PBMC from 6 healthy blood donors were examined in separate experiments. Each symbol represents one donor. *$p < 0.01$. (G, H) Comparison of chemokine (CCL2 and CXCL8) mRNA levels in EC after exposure of co-cultured A4 cells to NMO-IgG or control IgG. Total amount of CCL2 mRNA relative to total endothelial cell-selective adhesion molecule (ESAM) mRNA (G) or CXCL8 relative to ESAM (H) in each experiment was normalized to 1 using EC/A4 exposed to control IgG and reported as relative CCL2/ESAM or CXCL8/ESAM expression. Data are mean ± SEM with n = 5 replicates. *$p < 0.01$.

numbers of PBMC migrating under physiologic flow conditions across in vitro BBB cultures, as compared to reference conditions (EC/A co-cultures exposed to control IgG) (figure 2, E and F). Effects on transmigration were AQP4-dependent as demonstrated by additional controls: (1) EC/A co-cultures, in which astrocytes lack AQP4; (2) EC/A4 co-cultures exposed to control IgG. In these conditions, IgG had no observable effect on PBMC transmigration rates (figure 2, E and F). These results indicate that NMO-IgG engagement with abluminal astrocytic AQP4 produced signals that enhanced the ability of ECs to promote leukocyte transmigration under flow.

To address one potential mechanism underlying this effect, we examined levels of EC chemokine (CXCL1, 2, 8, 10, 12, CCL2, and CCL5) mRNAs by qRT-PCR, with results normalized to mRNA encoding for EC marker ESAM. In A4/EC co-cultures, signaling mediated by NMO-IgG in astrocytes selectively and significantly upregulated CCL2 and CXCL8 mRNA in EC (figure 2, G and H). These chemokines are expressed by cytokine-stimulated EC, and promote transmigration of monocytes and neutrophils, respectively.[20]

To address whether migration of selective PBMC subpopulations was enhanced in the presence of NMO-IgG, we performed transmigration assays under flow and assessed phenotypes of migrated cells by flow cytometry. Total numbers of migrated PBMC in EC/A4 co-cultures were significantly increased when A4 astrocytes were exposed to NMO-IgG prior to the assay (figure 3A). Postmigration phenotyping showed interindividual variation in the migration of PBMC subpopulations. These results were confirmed by evaluation of relative migration indices (figure 3B), which demonstrated a robust and significant increase in transmigration rates, but without a selective effect on a single subpopulation. It is worth noting that CCL2 signals both to monocytes and memory CD4+ and CD8+ T cells, potentially accounting in part for the increased migration of several PBMC populations.

Pathways by which NMO-IgG signaling to astrocytes stimulates EC. We hypothesized that soluble factors secreted by astrocytes might mediate the modulation of endothelial barrier functions in NMO-IgG-exposed EC/A4 co-cultures. In pilot studies, we assayed mRNA levels for 4 cytokines (IL-1β, IL-4, IL-6, IFN-β), 10 chemokines (CCL2, CCL5, CCL7, CCL8, CCL20, CXCL1, CXCL8, CXCL10, CXCL12, CX3CL1), and 5 vascular-targeted growth factors (TGF-β, VEGF, PDGF, BDNF, GDNF) using qRT-PCR in A4 or A monocultures incubated with NMO-IgG (figures e-2 and e-3). IL-6 was found to be significantly upregulated by NMO-IgG in A4. None of the factors we examined was affected by NMO-IgG in control A cultures or by control IgG in either A4 or A cells. Using ELISA, we confirmed and extended initial results by showing that NMO-IgG selectively induced IL-6 protein in A4 but not A cells (figure 4A).

As astrocyte expression of IL-6 in vivo was associated with BBB impairment in transgenic mice,[21] it was plausible that IL-6 might account for effects observed with abluminal exposure of EC/A4 co-cultures to NMO-IgG. Because EC do not express the transmembrane IL-6 binding receptor,[22,23] we incubated EC with IL-6/sIL-6R complexes, which trans-signals by associating with ubiquitous membrane gp130. Exposure to IL-6/sIL-6R complexes reduced Claudin 5 mRNA levels (figure 4B), increased BBB permeability to 10k dextran (figure 4C), increased CCL2 and CXCL8 mRNAs (figure 4D), and enhanced PBMC transmigration under flow (figures 4E and e-4A). NMO-IgG-mediated enhancement of PBMC transmigration under flow was abrogated when IL-6 receptor was neutralized by CD126 antibodies specific for IL-6 receptor α-chain (figures 4F and e-4B).

DISCUSSION While AQP4 antibodies are predominantly but not exclusively produced in the periphery, as indicated by molecular characterization of the immunoglobulin transcriptome and proteome[24] and by the peripherally acting agent tocilizumab,[25] their pathogenic effects in NMO are exerted within the CNS. Our data suggest that peripheral AQP4 antibodies contained in NMO-IgG access the intrathecal compartment behind the BBB in part through the action of a non-AQP4 endothelial-specific immunoglobulin, which increases BBB permeability (F.S., B.O., Y.T., R.M.R., unpublished observations). The present study, however, was designed to specifically elucidate the effects of AQP4 antibodies towards astrocyte maintenance of the BBB, immediately after those antibodies had crossed the BBB.

Our co-culture model of the BBB employed human EC and AQP4-positive or -negative astrocyte cell lines, and we used human IgGs derived from patients with NMO and controls. This particular experimental system is more reproducible and enables mechanistic studies. Potential limitations of our astrocyte cell lines include loss of elements of the primary-cultured astrocyte phenotype as they lose their physical connection with other CNS cells when cultured in a dish. For example, we observed that A cells express AQP4 mRNA, but protein levels were below the limit of detection in monoculture. Only when A cells were transfected to overexpress AQP4, as such designated A4 cells, AQP4 could be detected on the protein level and expression levels were preserved despite repeated passaging of cells.[18] However,

Figure 3 **Effects of abluminal neuromyelitis optica (NMO)–immunoglobulin G (IgG) on numbers and phenotypes of migrated peripheral blood mononuclear cells (PBMC)**

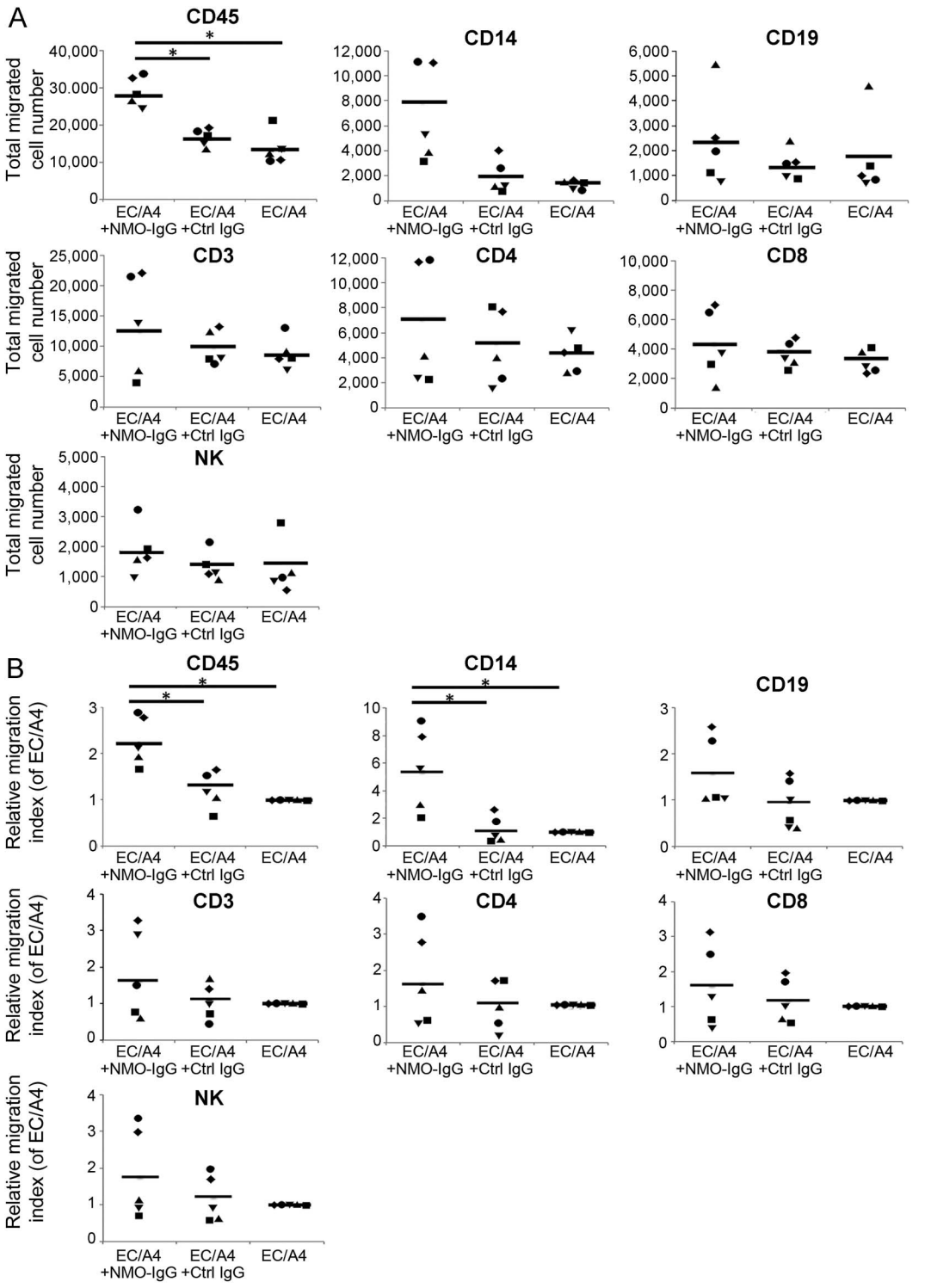

(A, B) PBMC from 5 different blood donors were subjected to transmigration assays under flow using endothelial cell (EC)/A4 co-cultures, which were abluminally exposed to NMO-IgG, control IgG, or no human IgG prior to the assay. Total migrated cells were counted, and migrated cells were phenotyped by flow cytometry. Total numbers (A) and migration indices (B) of distinct PBMC subpopulations were calculated by correlating percentages out of total PBMC (CD45+) determined by flow cytometry to total numbers of migrated cells. (A) Comparison of total numbers of migrated cells in total PBMC (CD45+), CD14+, CD19+, CD3+, CD4+, CD8+, and natural killer (NK) (CD3−, CD8dim, CD16+ CD56+) cells. (B) Comparison of relative migration indices in total PBMC (CD45+), CD14+, CD19+, CD3+, CD4+, CD8+, and NK cells. Migrated cell numbers in each experiment and for each subpopulation were normalized to 1 by reference to non-IgG-exposed EC/A4. Each symbol represents one donor. *$p < 0.01$.

Figure 4 **Effects of interleukin (IL)-6 trans-signaling in endothelial cells (EC)**

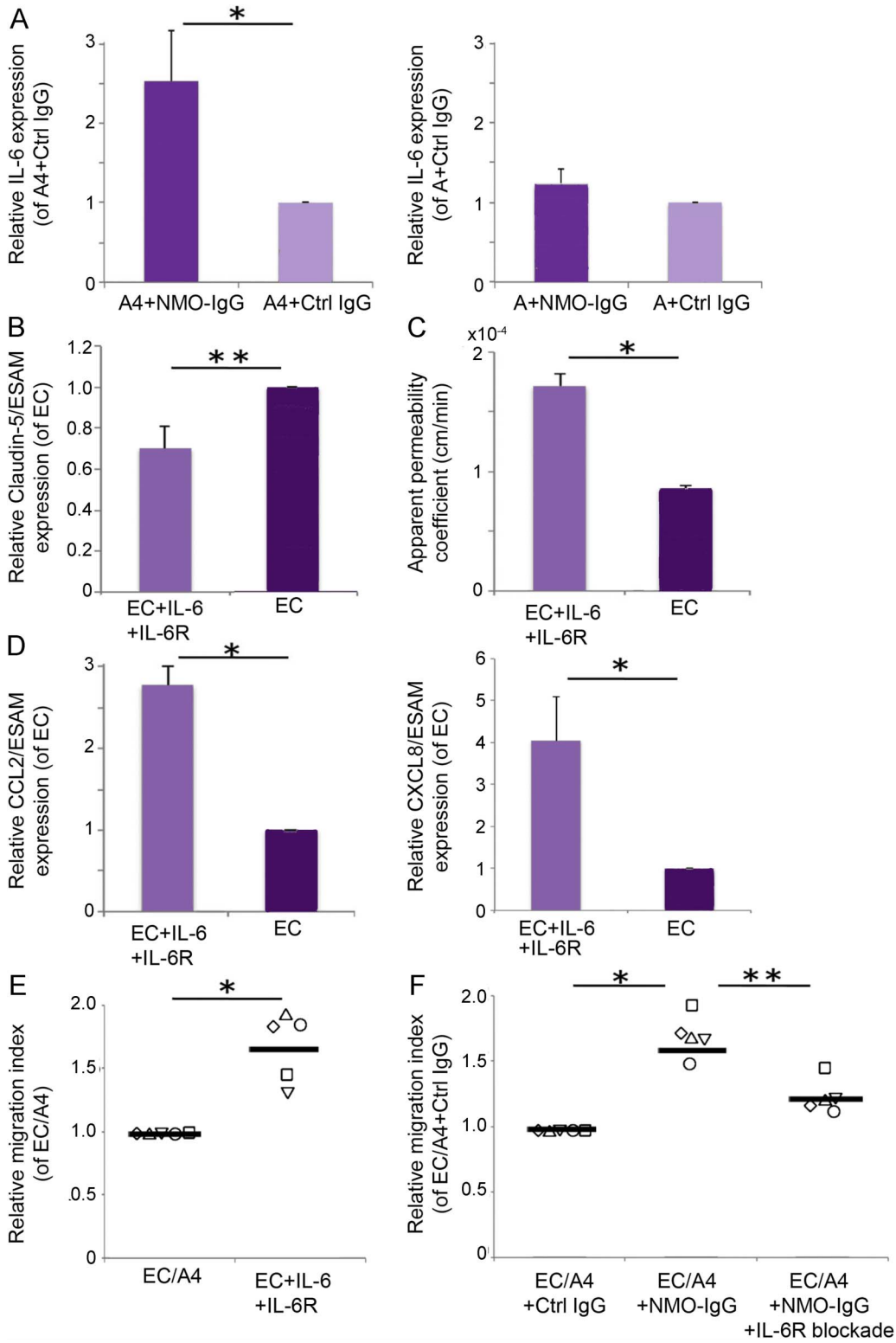

Outcome variables for each experiment shown in the figure were normalized as appropriate for the assay and cell type. For readability, normalization strategies are presented together at the end of this paragraph. (A) Neuromyelitis optica (NMO)–immunoglobulin G (IgG) selectively induced IL-6 protein expression in A4 (left panel) but not in A (right panel). Data are reported as normalized IL-6 expression and show mean ± SEM with n = 5 replicates. *$p < 0.01$. (B) Comparison of normalized Claudin 5 mRNA expression in EC in the presence or absence of IL-6/soluble interleukin-6 (sIL-6) receptor. Data are mean ± SEM with n = 5 replicates. **$p < 0.05$. (C) Effect of IL-6 trans-signaling on solute permeability with dextran 10k. Data are mean ± SEM with n = 5 replicates. *$p < 0.01$. (D) CCL2 (left panel) and CXCL8 (right panel) normalized mRNA expression in EC upon stimulation with IL-6/sIL-6 receptor. Data are

Continued

regardless of using conditionally immortalized or primary astrocyte cultures, results require validation in vivo using analysis of tissue from patient samples.

Our results carry translational potential. Exposure of NMO-IgG to the abluminal side of EC/astrocyte co-cultures substantially modified barrier properties of EC, acquiring an activated phenotype. BBB dysfunction along with IL-6 induction, caused by individual AQP4 antibody-positive sera, has been reported previously.[13,17,18] In seeking a mechanism for these effects, we found that NMO-IgG binding to astrocyte AQP4 selectively induced AQP4 internalization and production of IL-6. At this time, it remains elusive whether AQP4 internalization triggers downstream signaling pathways that induce IL-6 production in astrocytes, or whether these observations are not directly linked. Blocking IL-6 signaling removed the stimulatory effect of A4 cell exposure to NMO-IgG, whereas inducing IL-6 signaling in ECs was sufficient to mediate downstream consequences of abluminal NMO-IgG for astrocyte/EC co-cultures. These observations are consistent with reports that astrocytes express IL-6 in neuroinflammation[26] and that IL-6 downregulates EC tight junction molecules,[27] decreases barrier function,[28,29] and induces CCL2 and CXCL8.[30,31] In vitro, increased barrier permeability and enhanced leukocyte migration can also be induced via complement-dependent astrocytopathy, a mechanism associated with destructive lytic lesions in patients.[12,13] BBB dysfunction mediated by AQP4 internalization and the inflammatory phenotype of astrocytes as described here is complement-independent and we speculate that this mechanism is distinct and relates to sublytic lesions in patients. Endothelial cells do not express transmembrane IL-6 binding receptor, but higher levels of sIL-6R in CSF from patients with NMO were also observed,[32] suggesting that abundant intrathecal sIL-6R in patients with NMO is available for complexing with IL-6 in the course of pathogenesis.

The sources of IL-6 in vivo in NMO remain undetermined. Certainly, peripheral sources of IL-6 are important for disease pathogenesis as revealed by the therapeutic trials using tocilizumab[25,33] and the potential prediction of disease severity by measuring plasma IL-6 levels.[34] Of note, IL-6 receptor blockade has been reported as a promising strategy to reduce NMO attack frequency.[25,33,35,36] The results we present suggest a potential amelioration of attack severity as well.

AUTHOR CONTRIBUTIONS

Yukio Takeshita designed and performed the experiments, analyzed and interpreted the data, and wrote the article. Birgit Obermeier performed experiments, analyzed data, and revised the manuscript for content. Anne C. Cotleur analyzed the data and revised the manuscript for content. Simona F. Spampinato performed experiments and analyzed data. Fumitaka Shimizu and Erin Yamamoto confirmed reproducibility of experiments and analyzed data. Yasuteru Sano created cell lines and provided input for experimental design. Thomas J. Kryzer and Vanda A. Lennon provided NMO-IgG and control IgG as well as input for detailed experimental design. Takashi Kanda created cell lines and provided input for experimental design. Richard M. Ransohoff conceptualized the in vitro BBB models and this research, designed the experiments, analyzed the data, and wrote the article.

STUDY FUNDING

Supported by Guthy Jackson Charitable Foundation, NIH (K24NS51400, R21NS78420, and P50NS38667, Project 1 to Richard M. Ransohoff), and Japan Society for the Promotion of Science (JSPS) (JP16K19513).

DISCLOSURE

Y. Takeshita reports no disclosures. B. Obermeier is employed by Biogen. A.C. Cotleur is employed by Biogen. S.F. Spampinato reports no disclosures. F. Shimizu was employed by Biogen. E. Yamamoto, Y. Sano, and T.J. Kryzer report no disclosures. V.A. Lennon received royalties from RST/Kronus for sale of aquaporin-4 autoantibody testing kits and for commercial aquaporin-4 autoantibody testing performed outside Mayo Clinic; received research support from NIH; and has a potential financial interest in aquaporin-4 as an aid for cancer diagnosis. T. Kanda is editor-in-chief of *Clinical and Experimental Neuroimmunology*; is on the editorial board for *Neuropathology*; and received research support from Japan Society for the Promotion of Science. R.M. Ransohoff serves on the scientific advisory board for Chemocentryx; received travel funding and/or speaker honoraria from Biogen Idec and Novartis; special guest and speaker, Max-Planck Institute Retreat Ringberg Germany, 2009; invited plenary speaker, 1st Keystone Symposium on MS, Santa Fe, New Mexico, 2009; Grand Rounds in Neurology, Johns Hopkins University, Baltimore, MD, 2009; Keynote Lecture, Opening of Neuropathology Institute, Freiburg, Germany, 2009; Plenary Lecture, Kick-off meeting for Neurodegeneration Research Center, Bonn, Germany, 2009; invited seminar, Institute for Research in Biomedicine, Bellinzona, Switzerland, 2009; invited speaker, FDA/NYAS Conference: "Cytokine Therapies," New York, 2009; invited external speaker, "Annual Japanese MS Workshop," Kyushu, Japan, 2009; visiting professor, Department of

Figure 4 legend, continued:
mean ± SEM with n = 5 replicates. *$p < 0.01$. (E) Effect of IL-6 trans-signaling on transmigration of peripheral blood mononuclear cells (PBMC) across the in vitro blood–brain barrier under flow. PBMC from 5 different blood donors were examined in separate experiment. Each symbol represents one donor. Data are presented as relative migration index. *$p < 0.01$. (F) Effects of IL-6R blockade on migrated cell numbers. PBMCs from 5 different blood donors were examined in separate experiments. Each symbol represents one donor. Data are presented as relative migration index. *$p < 0.01$. (E, F) See figure e-2 for corresponding total numbers of migrated cells. Normalization: (A) Total IL-6 in each experiment was normalized to 1 using A4 exposed to control IgG (left panel) or A exposed to control IgG (right panel), respectively, and is reported as relative IL-6 expression. (B) Total amount of Claudin 5 relative to ESAM in each experiment was normalized to 1 using untreated EC and reported as relative Claudin 5/ESAM expression. (D) Total amount of CCL2 relative to ESAM or CXCL8 relative to ESAM in each experiment was normalized to 1 using untreated EC and reported as relative expression of CCL2/ESAM (left panel) or CXCL8/ESAM (right panel), respectively. (E) Total migrated cell numbers in each experiment were normalized to 1, which is represented by untreated EC/A4 co-cultures and data are reported as relative migration index. (F) Total migrated cell numbers in each experiment were normalized to 1 which was represented by EC/A4 co-cultures exposed to control IgG and data are reported as relative migration index.

Neurology, Kyushu University, Fukuoka, Japan, 2009; consultant, Nature "Landscape" editorial meeting on neuroimmunology, 2009; invited seminar, GSK Hammersmith Hospital, London, 2009; invited speaker, 12th International Symposium, "Signaling at the BBB," London, England, 2009; co-organizer/speaker, "Chemokines and Chemokine Receptors in the CNS," Rome, 2009; Grand Rounds in Neurology, Ottawa General Hospital, Ontario, Canada, 2009; invited speaker, Keystone Symposium "Alzheimer's Disease," Colorado, 2010; NIH EUREKA Review IRGs, 2008–2010; invited speaker, ASN annual meeting, Santa Fe, 2010; invited speaker, Nikolas Histiocytosis-X Symposium, Athens, Greece, 2010; invited speaker, FOCIS 2010 Symposium, "Interventional Immunology," Boston, 2010; keynote speaker, Neuroimmunology Symposium, Kyoto, Japan, 2010; workshop chair, International Congress of Immunology, Kobe, Japan, 2010; Plenary Lecture, PACTRIMS, Bali, Indonesia, 2010; symposium organizer and chair, ANA annual meeting, San Francisco, CA, 2010; workshop chair, Special Interest Groups, ANA, San Francisco, CA, 2010; invited speaker, Theodor Kocher Institute, Bern, Switzerland, 2010; invited speaker/session chair, Cell Press Symposium "Inflammation in Disease," Lisbon, 2010; invited speaker, Brazilian Society of Pharmacology 42nd annual meeting, Brazil, 2010; external reviewer, DFG "Centers of Excellence" Applications, Frankfurt, Germany, 2011; invited speaker, AAAS/Abelson Symposium "Defeating AD," Washington, DC, 2011; is on the editorial board for *Neurology® Neuroimmunology & Neuroinflammation*; consulted for Pfizer Teva; received research support from Chemocentryx, Biogen, and National MS Society; and holds stock or stock options in SAB, Chemocentryx, and Biogen. Go to Neurology.org/nn for full disclosure forms.

Received August 6, 2016. Accepted in final form November 2, 2016.

REFERENCES

1. Wingerchuk DM, Lennon VA, Lucchinetti CF, et al. The spectrum of neuromyelitis optica. Lancet Neurol 2007;6: 805–815.
2. Misu T, Hoftberger R, Fujihara K, et al. Presence of six different lesion types suggests diverse mechanisms of tissue injury in neuromyelitis optica. Acta Neuropathol 2013; 125:815–827.
3. Devic E. Subacute myelitis complicated by optic neuritis. Bull Med 1894;8:1033–1034.
4. Cree BA, Goodin DS, Hauser SL. Neuromyelitis optica. Semin Neurol 2002;22:105–122.
5. Lucchinetti CF, Mandler RN, McGavern D, et al. A role for humoral mechanisms in the pathogenesis of Devic's neuromyelitis optica. Brain 2002;125: 1450–1461.
6. Lennon VA, Wingerchuk DM, Kryzer TJ, et al. A serum autoantibody maker of neuromyelitis optica: distinction from multiple sclerosis. Lancet 2004;364: 2106–2112.
7. Saiz A, Zuliani L, Blanco Y, et al. Revised diagnostic criteria for neuromyelitis optica (NMO) application in a series of suspected patients. J Neurol 2007;254:1233–1237.
8. Rash JE, Yasumura T, Hudson CS, et al. Direct immunogold labeling of aquaporin-4 in square arrays of astrocyte and ependymocyte plasma membranes in rat brain and spinal cord. Proc Natl Acad Sci USA 1998;95:11981–11986.
9. Lennon VA, Kryzer TJ, Pittock SJ, et al. IgG marker of optic-spinal multiple sclerosis binds to the aquaporin-4 water channel. J Exp Med 2005;202:473–477.
10. Howe CL, Kaptzan T, Magaña SM, et al. Neuromyelitis optica IgG stimulates an immunological response in rat astrocyte cultures. Glia 2014;62:692–708.
11. Magaña SM, Matiello M, Pittock SJ, et al. Posterior reversible encephalopathy syndrome in neuromyelitis optica spectrum disorders. Neurology 2009;72:712–717.
12. Hinson SR, Pittock SJ, Lucchinetti CF, et al. Pathogenic potential of IgG binding to water channel extracellular domain in neuromyelitis optica. Neurology 2007;69: 2221–2231.
13. Vincent T, Saikali P, Cayrol R, et al. Functional consequences of neuromyelitis optica-IgG astrocyte interactions on blood-brain barrier permeability and granulocyte recruitment. J Immunol 2008;181:5730–5737.
14. Obermeier B, Daneman R, Ransohoff RM. Development, maintenance and disruption of the blood-brain barrier. Nat Med 2013;12:1584–1596.
15. Takeshita Y, Obermeier B, Cotleur A, et al. An in vitro blood-brain barrier model combining shear stress and endothelial cell/astrocyte co-culture. J Neurosci Methods 2014;232:165–172.
16. Sano Y, Shimizu F, Abe M, et al. Establishment of a new conditional immortalized human brain microvascular endothelial cell line retaining an in vivo blood-brain barrier function. J Cell Physiol 2010;225:519–528.
17. Shimizu F, Sano Y, Takahashi T, et al. Sera from neuromyelitis optica patients disrupt the blood-brain barrier. J Neurol Neurosurg Psychiatry 2012;83:288–297.
18. Haruki H, Sano Y, Shimizu F, et al. NMO sera down-regulate AQP4 in human astrocyte and induce cytotoxicity independent of complement. J Neurol Sci 2013;331:136–144.
19. Hinson SR, Romero MF, Popescu BF, et al. Molecular outcomes of neuromyelitis optica (NMO)-IgG binding to aquaporin-4 in astrocytes. Proc Natl Acad Sci USA 2012; 109:1245–1250.
20. Takeshita Y, Ransohoff RM. Inflammatory cell trafficking across the blood-brain barrier: chemokine regulation and in vitro models. Immunol Rev 2012;248:228–239.
21. Vallieres L, Campbell IL, Gage FH, et al. Reduced hippocampal neurogenesis in adult transgenic mice with chronic astrocytic production of interleukin-6. J Neurosci 2002;22: 486–492.
22. Saito M, Yoshida K, Hibi M, et al. Molecular cloning of murine IL-6 receptor-associated signal tranducer, gp130, and its regulated expression in vivo. J Immunol 1992;148: 4060–4071.
23. Jones SA, Horiuchi S, Topley N, et al. The soluble interleukin 6 receptor: mechanisms of production and implications in disease. FASEB J 2001;15:43–58.
24. Kowarik MC, Dzieciatkowska M, Wemlinger S, et al. The cerebrospinal fluid immunoglobulin transcriptome and proteome in neuromyelitis optica reveals central nervous system-specific B cell populations. J Neuroinflammation 2015;12:19.
25. Araki M, Matsuoka T, Miyamoto K, et al. Efficacy of the anti-IL-6 receptor antibody tocilizumab in neuromyelitis optica: a pilot study. Neurology 2014;82:1302–1306.
26. Gruol DL, Nelson TE. Physiological and pathological roles of interleukin-6 in the central nervous system. Mol Neurobiol 1997;15:307–339.
27. Cohen SS, Min M, Cummings EE, et al. Effects of interleukin-6 on the expression of tight junction proteins in isolated cerebral microvessels from yearling and adult sheep. Neuroimmunomodulation 2013;20:264–273.
28. Maruo N, Morita I, Shirau M, et al. IL-6 increases endothelial permeability in vitro. Endocrinology 1992;131: 710–714.
29. Desai TR, Leeper NJ, Hynes KL, et al. Interleukin-6 causes endothelial barrier dysfunction via the protein kinase C pathway. J Surg Res 2002;104:118–123.

30. Romano M, Sironi M, Toniatti C, et al. Role of IL-6 and its soluble receptor in induction of chemokines and leukocyte recruitment. Immunity 1997;6:315–325.
31. Modur V, Li Y, Zimmerman GA, et al. Retrograde inflammatory signaling from neutrophils to endothelial cells by soluble interleukin-6 receptor alpha. J Clin Invest 1997; 100:2752–2756.
32. Wang H, Wang K, Zhong X, et al. Notable increased cerebrospinal fluid levels of soluble interleukin-6 receptors in neuromyelitis optica. Neuroimmunomodulation 2012;19:304–308.
33. Ringelstein M, Ayzenberg I, Harmel J, et al. Long-term therapy with interleukin 6 receptor blockade in highly active neuromyelitis optica spectrum disorder. JAMA Neurol 2015;72:756–763.
34. Barros PO, Cassano T, Hygino J, et al. Prediction of disease severity in neuromyelitis optica by the levels of interleukin (IL)-6 produced during remission phase. Clin Exp Immunol 2016;183:480–489.
35. Krumbholz M, Meinl E. B cells in MS and NMO: pathogenesis and therapy. Semin Immunopathol 2014;36:339–350.
36. Ayzenberg I, Kleiter I, Schröder A, et al. Interleukin 6 receptor blockade in patients with neuromyelitis optica nonresponsive to anti-CD20 therapy. JAMA Neurol 2013;70:394–397.